LUND UNIVERSITY
Faculty of Science

Construction and Characterization of a Confocal Setup for Functionalization of Light Emitting Diodes and Laser Diodes Using an Amorphous Nonlinear Medium

Hana Zeneli

Thesis submitted for the degree of Bachelor of Science
Project duration: 2 months

Supervised by Nils Rosemann and Rasmus Westerström

Department of Physics
Division of Synchrotron Radiation

May 2018

Abstract

A confocal microscope is built to examine molecular powders, and in particular the $(PhSn)_4 S_6$ cluster, that emits white light when irradiated with infrared laser light. The confocal microscope operating at long working distances is assembled and characterized. The components of the setup are first chosen according to requirements of the planned experiment. Thereafter, the microscope is assembled and aligned. Subsequently, the microscope is tested regarding the realized laser spot size, calibration, field of view, magnification and laser throughput.

Following the characterization of the setup, a brief test is performed using a thin layer of $(PhSn)_4 S_6$ cluster molecules deposited via laser deposition. This layer is then examined regarding its nonlinear optical properties.

Contents

1 Introduction **3**

2 Theoretical Background **7**

2.1 Light matter interaction and nonlinear optics 7

2.2 Amorphous nonlinear medium 10

2.3 Requirements on the confocal microscope 11

2.4 Magnification and field of view of a microscope 14

2.5 Resolution of a microscope 15

2.6 Laser beam properties 15

3 Experiments **17**

3.1 Assembly of the microscope setup 17

3.2 Calibration 19

3.3 Laser spot size 20

3.4 Laser throughput 21

4 Results **23**

4.1 Calibration 23

4.2 Field of view 23

4.3 Laser spot size 24

4.4 Laser throughput 25

4.5 Laser deposition of the amorphous nonlinear medium 26

5 Outlook **28**

5.1 Summary 28

1 Introduction

Lasers are versatile light sources with unique properties. The laser was first invented in 1960 by Maiman et al. [1]. Since then new lasers are constantly evolving, which makes the potential improvements of the laser's techniques interesting to study more closely.

The name LASER is an acronym and stands for Light Amplification by Stimulated Emission of Radiation [2, 3]. Lasers possess characteristics such as having intense monochromatic light and emitting a collimated beam of coherent light [4]. Lasers have gained widespread popularity in terms of application in physics and other sciences due to these unique properties. The laser was first reported in 1960 by Maiman et al. Lasers have since then risen in research, serving in many different applications within industry and the medical field. Today lasers have reached the commercial market and are implemented in several every day items, such as DVD-players and distance meters in cars [5].

Despite the numerous benefits due to the properties of laser light, some of them can be a disadvantage depending on the targeted application. Thus, the search for new sources of laser light continues. For example, having monochromatic light can be of an inferior favor, depending on the application, i.e. illuminating a room with only one wavelength might not be practical. This disadvantage is caused by the active material, also referred to as the gain medium. The active material restricts the laser to work only in a certain wavelength region. Overcoming this limitation is possible with e.g. second harmonic generation (SHG). This is a technique that was first presented a year after the invention of the laser, a project led by the late Peter Franken [6]. Franken et al. demonstrated that second harmonic generation of a pulsed ruby laser i.e. can convert the 694nm (red) emission of a ruby crystal

into 347nm (blue/ultraviolet). This was the gateway into the field of nonlinear optics. In the mid-1960's a multitude of other nonlinear processes were discovered [6].

With the newly found understanding for the field of laser physics and nonlinear optics and the increasing laser intensity, came discoveries of new phenomena like supercontinuum (SC) generation. SC generation was first discovered in bulk glass by Alfano and Shapiro [4]. In supercontinuum generation, a high intensity laser of one colour is used to generate a broad spectrum with laser like properties, in other words white laser light [7]. Supercontinuum generation is a phenomena with many diverse applications, some of them being the field of spectroscopy, pulse compression, and the design of tunable ultrafast femtosecond laser sources [8]. The supercontinuum can be generated in different types of materials. The material of choice is usually gas, plasma, photonic crystal fibers or specially designed nanostructures. These materials are specially designed to promote SC. For SC generation to occur in these materials high laser intensities are needed, but these intensities are still fairly low in comparison to the ones needed in glass. The general disadvantage of these types of active materials is that all of them demand high laser powers.

Quite recently it was shown that in an amorphous material consisting of tin-sulfur clusters supercontinuum generation can be observed even for comparably low laser intensities [9, 10]. This possibly opens the way for further applications of lasers (e.g. optical coherence tomography (OCT) and pointed illumination like in a projector or head up display). The underlying process of supercontinuum generation in that material, however, is to this date not completely understood. Furthermore, the handling of the setups, i.e. confocal microscopes, used for experiments dealing with nonlinear optics (e.g. SC generation) have potential of improvement. This

will be the aim of this project. This thesis will later act as a guide to characterizing a confocal microscope setup. In the future this microscope will be used to functionalize laser diodes and high-power light emitting diodes (LEDs) with the nonlinear medium.

A confocal microscope setup operating at long distances is planned and assembled. The setup is then characterized. The various parameters characterized are the spot size, the intensity of the laser spot in the sample position, the field of view, magnification, and the calibration. Thereafter, a first test of simple laser deposition is performed.

By having this low cost infrared laser pointer that transforms into white light it would work as a terrific substitute to more expensive methods. In the long run, replacing older and more expensive methods by lower-cost one which uses low-intensity white light would result in making some fields and research areas in science more affordable. This implies that more research can be done since there would be more money to cover this, which should be considered to be of great importance. Performing more research in different fields, in this case physics, leads to an increased understanding of the world and the environments surrounding us. By understanding our surroundings we can also contribute to making changes and improving them. Performing experiments and measurements with a setup like the one built for this project would also reduce the size of current setups substantially. Thus, the need of having access to large lab spaces would no longer be an issue the same way it is when needing the larger lasers for the experiments. If the white light generation seems promising after further studies have been performed, this new method and material could potentially substitute older, more energy demanding ones. Lower costs and smaller setups implies more convenience. Because of white light's many applications within physics and optical instruments, its potential

improvements are vital for research to move forward and become more stable, economically sustainable and also simplified.

This thesis will in the second chapter give insight on the basic theoretical background required for the project. This background theory will consist of basics in nonlinear optics and a short description of the nonlinear material. A brief description of the nonlinear light-matter interaction will be given in this chapter. Thereafter, the setup planning is discussed. The design of the setup will be addressed, i.e. what is required and why it is required. The third section describes the assembly of the setup in more detail. It also gives an overview of how the setup is tested on whether the previously defined requirements are reached. In the fourth section the results of the tests and also the results of the first laser deposition test are presented. And finally in section 5 the thesis is summed up and an outlook on the further development is given.

2 Theoretical Background

This chapter will give the theoretical background needed for performing the experiment and characterization of the microscope. Basic theory on nonlinear optics and the nonlinear material will be explained. Thereafter the chapter will continue on discussing the characterization of the setup including several aspects. Different properties of the laser and setup are of interest, i.e the intensity, spot size, magnification, field of view and calibration.

2.1 Light matter interaction and nonlinear optics

We can see the world around us due to the fact that light interacts with matter. This interaction can lead to various results, i.e. light can be absorbed, transmitted, reflected or scattered. All of these processes are well described in theoretical manners. In the book Semiconductor Optics (Klingshirn, C. F., 2012) absorption of light is described as "the transformation of the energy of the light field into other forms of energy like heat, chemical energy or electromagnetic radiation which is not coherent and generally also frequency shifted with respect to the incident beam" [11].

Depending on the form of interaction, some descriptions are making use of the electromagnetic-wave nature of light, while others are described by the particle (i.e. photon) like nature of light. This thesis will mainly focus on the wave-like behaviour of light. For a more detailed discussion of light matter interaction and nonlinear optics, the reader is referred to textbooks on this topic (for example [6], [12], [13]).

The basic description of electromagnetic waves is given by Maxwell's equations.

Maxwell's equations are an indication of how charges produce fields [14].

Maxwell's equations are given as:

$$\nabla \cdot E = \frac{1}{\epsilon_0}\rho \tag{1}$$

$$\nabla \cdot B = 0 \tag{2}$$

$$\nabla \times E + \frac{\partial B}{\partial t} = 0 \tag{3}$$

$$\nabla \times B - \mu_0\epsilon_0\frac{\partial E}{\partial t} = \mu_0 J \tag{4}$$

The first equation is Gauss's law. The second equation is Gauss's law for magnetic fields. It states that the magnetic flux through a closed surface is zero, this infers that no magnetic monopoles exist. The third is called Faraday's law, once the electric field E and magnetic field B are not separated. The same thing applies to the fourth equation; if E and B are separated the equation is given as Ampere's law with Maxwell's correlation. The separation of the fields E and B to the left and the charges ρ and currents J to the right emphasizes that all electromagnetic fields are attributable to charges and currents.

An electric field gives rise to an oscillating polarization of the medium. The polarization constitutes the source of a oscillating electric field, where this new oscillating electric field is the white light emitted. In light matter interaction equation 5 is one of the most important. It can be directly derived from Maxwell's equations.

$$P(\omega, k) = \epsilon_0\chi^{(1)}(\omega, k)E(\omega, k) \tag{5}$$

where P is a macroscopic polarization and E is an oscillating electric field. ϵ_0 is the vaccuum permittivity, $\chi^{(1)}$ is the susceptibility, and ω and k are the frequency of the wave and its direction of propagation respectively. Assuming spatial homogeneity

of the material and time invariance, the polarization is expressed as in equation 5 [15].

For low field strength (i.e. below approximately $10^8 \frac{V}{\text{cm}}$) the formula 5 holds true [15, 16]. Whenever this is the case, it is referred to as linear optics. The induced polarization scales linearly with the electric field strength, hence the name. Linear optics describes a large variety of processes e.g. photoluminescence and absorption. In linear optics, light-matter interaction follows the rule of particle conservation, which implies that the number of particles is conserved. In photoluminescence for example: one photon gets absorbed, it excites one electron, that later emits one photon.

If the field strength increases, equation 5 no longer holds. In this case, higher order terms gain a higher relevance. The polarization has to be expressed in terms of higher orders through an expansion by a Taylor series as the following:

$$P = \epsilon_0 \Big[\chi^{(1)} E_1 + \chi^{(2)} E_1 E_2 + \chi^{(3)} E_1 E_2 E_3 + ... \Big] \tag{6}$$

where

$$E_i \mathrel{\hat{=}} E_i(\omega_i, k_i)$$

.

χ^2 and χ^3 are the second order and third order susceptibility, respectively. Higher order terms become important only after a certain threshold i.e. $10^8 \frac{V}{\text{cm}}$ (for atoms). As the susceptibility is a material constant, by designing a material in a certain way the susceptibility can be increased, thus the threshold for nonlinear effects can be decreased. In general, the electric field strength, or a combination between the electric field strength and the susceptibility, determines to which degree the power series has to be expanded [15].

Supercontinuum generation should in general be described by an endless Taylor

series because a broad range of components (wavelength) are involved. Thus, the perturbation approach in equation 6 is not practical. That is why the most common description of supercontinuum generation is done in terms of self phase modulation. Self phase modulation is related to the Kerr effect [4]. In non-linear light optics, the light-matter interaction behaves differently in the sense that it does not conserve the amount of particles. The most usual scenario is that more photons get in than out, e.g. in SHG where two low-energy photons get converted into one high-energy photon.

2.2 Amorphous nonlinear medium

The material investigated in this project is an amorphous powder consisting of cluster molecules, named 1,3,5,7-Tetrakis(4-phenyl)-2,4,6,8,9,10-hexathia-1,3,5,7-tetrastanna-adamantane ($(\mathrm{Ph\,Sn})_4\mathrm{S}_6$). This material is known to exhibit a strong nonlinear response when irradiated with infrared laser light. Other chemical compounds have also been found to produce white light when irradiated with infrared light [9]. The molecular structure of the compound investigated in this project is shown in figure 1. It consits of a adamantane like core made of tin and sulfur atoms that is surrounded by four phenylligands.

The field strength needed for the nonlinear white-light generation is given by the threshold of ~23 $\frac{V}{\mathrm{cm}}$, corresponding to a laser intensity threshold of ~0.7 $\frac{W}{\mathrm{cm}^2}$ [15]. Figure 2 illustrates the white light spectrum produced by the compound. It was found that the sample has to be kept in vacuum during white light generation. Apart from the threshold field strength, this has to be taken into account when designing a setup to work with the sample.

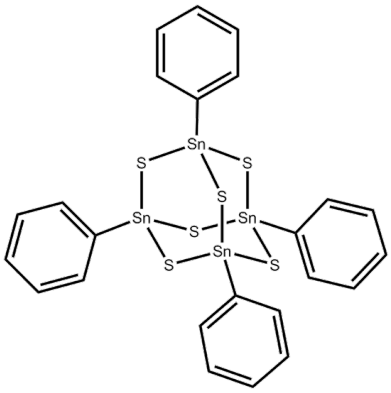

Figure 1: Molecular structure of the amorphous nonlinear medium of interest in this project [15].

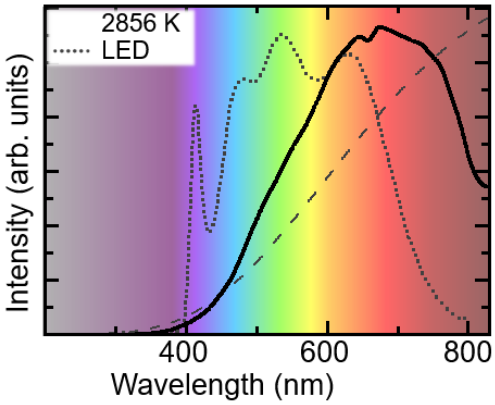

Figure 2: Graph of the white light spectrum. The left axis show the intensity of the light in arbitrary units, while the bottom axis show the wavelength in nm [15].

2.3 Requirements on the confocal microscope

Prior to the beginning of this thesis the key application of the planed microscope has been defined. It should be capable of producing white light using the previously described amorphous cluster compound. At the same time it should be able to image a LED and laser diode during operation. These requirements lead to the decision of building a confocal microscope. As described in the last sub-chapter

the sample defies some requirements on the planed microscope: for white light generation a threshold field strength of ~23 $\frac{V}{\text{cm}}$ has to be provided; additionally the sample has to be kept in vacuum. The former demands for either a high intensity laser or a spot size as small as possible, the latter, however, restricts the distance from the last optical element to the sample as a vacuum chamber intrinsically has a certain height. Further requirement for the planed setup arise from the fact that in a later stage it is planed to investigate LEDs and laser diodes with the setup. The size of the respective LEDs defines the minimum field of view, while the small size of the emitting part of a laser diode naturally demands to have a magnification as good as possible.

The demands for high magnification and small spot size would usually result in using a microscope objective. These objectives, however, have a low working distance. Whereas the working distance is defined as the distance from the last surface of the sample to the surface of the lens. This low working distance is not compatible with the restriction of a certain distance to the sample caused by the vacuum-chamber. In many cases this working distance equals the the focal length of the lens. For the setup in this experiment the working distance has to be at least 4 cm. This is due to the fact that the sample is placed approximately 1 cm below the glass window of the sample chamber.

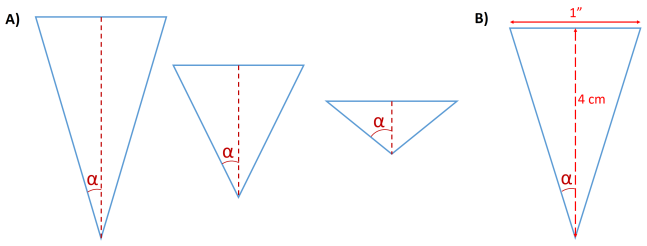

Figure 3: A) Illustration of the acceptance angle α for the light hitting the sample. B) Illustration of the NA for the setup.

The working distance is dependent on the acceptance angle α as the following:

$$\tan(\alpha) = \frac{\text{diameter of lens}}{\text{working distance}} \tag{7}$$

The numerical aperture NA is given as the following [17]:

$$\text{NA} = n \cdot \sin(\alpha) \tag{8}$$

where n is the refraction index, which in this experiment is $n = 1$ for air. A high value for 2α means a high numerical aperture. The smaller the acceptance angle α of the light coming in, the less bright the image gets. The angle fulfills the condition $2\alpha < 180°$.

Figure 3A illustrates the working distance and acceptance angle of the light on and from the sample. In figure 3B values needed for deriving the numerical aperture are given. Given the diameter of the lens (1 inch $\approx$ 2.54 cm) and the chosen working distance (4 cm) of the setup the numerical aperture for this setup is then calculated as the following:

$$\tan(\alpha) = \frac{1/2”}{4\text{cm}}$$

$$\Rightarrow \alpha = \arctan\left(\frac{0.01225 \text{ m}}{0.04 \text{ m}}\right) = 0.297 \tag{9}$$

$$\text{NA} = 1 \cdot \sin(\alpha) = 0.301 \tag{10}$$

To increase the numerical aperture for the setup, a larger lens could be used. By using a very large lens a high numerical aperture together with a high working distance could also be achieved. Using a lens with a smaller focal length would also contribute to increasing the NA, but decreasing the working distance. This alternative is possible to perform to a certain extent only, since a long working distance is in fact needed for the experiment.

2.4 Magnification and field of view of a microscope

There are different types of optical microscopes. The microscope setup assembled and used in our experiment is a confocal microscope. As the name implies, this microscope uses a confocal optical system. It consists of two lenses without image in between i.e. collimated beam in between the lenses [18].

The setup has parallel beams between objective lens and ocular lens. The focal length of the objective lens f_1 needs to be as small as possible in order for the magnification V to be as large as possible. This is given by formula 11 [19]. The focal length of the ocular lens is denoted f_2.

$$V = \frac{f_2}{f_1} \tag{11}$$

Because of the limited size of the setup the value for f_2 is also restricted in value. Two options were available for the focal length of the ocular lens, either 15 cm or 20 cm. These are chosen due to stock availability.

Other things that need to be considered are the size of the camera chip. The detector of the setup is a Microsoft HD Live Cam with a chip size of 4.5 x 3.5 mm. The chip size in combination with the magnification of the setup defines the field of view. The smallest possible f_1 is picked by choosing a value that allows for the beam spot to be as small as possible, and that yields a large enough working distance considering the vacuum chamber.

The setup will later be used to monitor LEDs and laser diodes. The targeted LEDs have a chip size of $\approx 1 \times 1$mm. This implies that the field of view should have the same size as a minimum requirement. An increased magnification decreases the field of view, which is important when looking on the LEDs, since the aim is to

observe the whole chip of the LED.

2.5 Resolution of a microscope

The theoretical resolution, or resolving power, of the setup is given by Abbe's diffraction formula for lateral resolution [17]:

$$\frac{\lambda}{2 \cdot \mathrm{NA}}$$

where λ denotes the wavelength of the laser. The resolution should be given in the nanometer range. The pixels are too large to resolve objects in this range, since the magnification is too low. This is the underlying reason to as why the resolution in practice is not the same as the theoretical value for the resolution.

2.6 Laser beam properties

The laser beam spot is usually described by a Gaussian curve. This is due to the intensity of a Gaussian beam being described as:

$$I = I_0 \cdot e^{-\frac{2r^2}{w^2}} \tag{12}$$

where I is the intensity at a certain distance from the center, I_0 is the maximum intensity at the center of the beam, r is the radial distance from the center of the beam, and w is the half width of the beam. [20]

The field strength E is correlated to the intensity I and can be derived from the following formula [12]:

$$I = \frac{1}{2}\epsilon_0 c E^2 \tag{13}$$

where ϵ_0 is the vacuum permittivity and c is the speed of light.

Having only knowledge of the power of the laser of interest is not very useful in many cases. For example, it does not take the area of the laser spot into consideration at all. A laser with a low power but small spot area can cause more harm on e.g. human skin than a high power laser with a large beam spot. By taking the area into consideration and instead knowing the intensity of the laser, rather than the power, it is easier to estimate the level of danger when handling the laser.

3 Experiments

Confocal microscopy is a method often used and applied within life sciences, semiconductor inspections and material sciences. This chapter will discuss the assembly of the setup and the experiments later performed with this setup. This chapter will also treat the characteristics of the laser, i.e. the power, the spot size of the laser beam, the calibration, and how these qualities were characterized. Lastly, a brief description on the performed laser deposition is given.

3.1 Assembly of the microscope setup

A sketch of the final microscope setup is given in fig. 4. The infrared light emitted from the laser is first reflected off of two mirrors towards a beam splitter. The beam splitter reflects light with a wavelength longer that 900nm, while light with a shorter wavelength is transmitted through. Thus, the infrared light is directed towards the objective lens that is in front of the sample chamber and focuses the laser onto the sample. The sample will generate a spot of white light once irradiated with the infrared laser. This white light is collimated by the objective lens and then reflected towards the beam splitter and passes through it. Residual scattered laser light is also collimated by the objective lens and directed towards the beam splitter, although it gets reflected rather than passing through. The emitted sample light then travels through two coated filters before it reaches the detector. These two coated filters are placed before a detecting system to eliminate the last traces of infrared light that might otherwise pass through to the detector. An additional ocular lens is placed in the beam path that creates the image of the sample on the detector chip. The detector is a standard complementary metal oxide sensor (CMOS) as it can be found in e.g. webcams, which is read out by a

computer that is used to both display as well as save images of the sample.

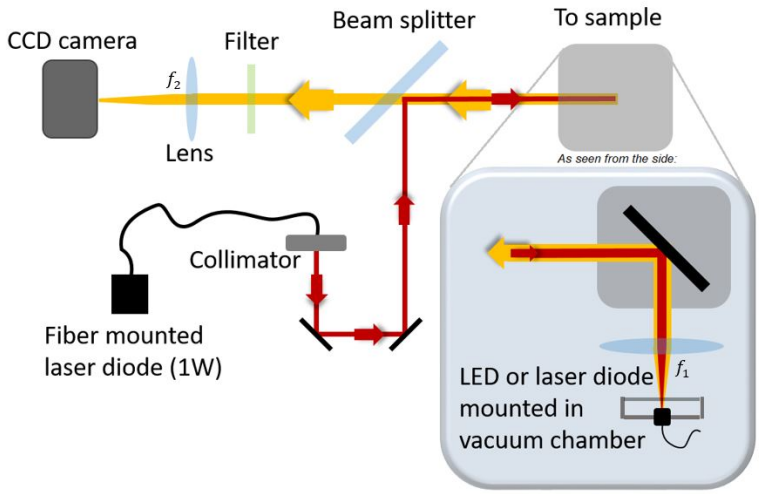

Figure 4: Sketch of setup adapted from reference [21].

As mentioned in the chapter 2.4, the focal length of the objective lens is determined by the geometry of the setup, and is chosen to be 4 cm due to convenience. This allows a large enough distance between the lens and sample without interfering with the vacuum chamber. Two options were then available for the focal length of the ocular lens, either 15 cm or 20 cm.

The most optimal focal length for a lens to use in this setup is found by calculating the value for when the field of view is exactly the same size as the chip of the camera, namely 4.5 x 3.5 mm. This would yield the best suitable value for the magnification. Thereafter the value for the optimal focal length for the ocular lens[1] can be found.

$$f_2 = 15 \text{ cm} \Rightarrow V = 3.75 \Rightarrow \text{Field of view} = 1.2 \times 0.93 \text{ mm}$$

$$f_2 = 20 \text{ cm} \Rightarrow V = 5 \Rightarrow \text{Field of view} = 0.9 \times 0.7 \text{ mm}$$

[1] f_2 in equation 11

The ideal focal length to match the field of view to the size of the LED chip (1× 1 mm) would be somewhere in between 15 cm and 20 cm. Since there are no lenses with such a specific focal length, the one chosen for this experiment is the most optimal possible, which is 15 cm.

3.2 Calibration

The optical system images a magnified picture of the sample onto the camera chip. This image is detected by pixels of a fixed size. Due to the fixed size, each pixel monitors a certain area of the image. As the pixels are squared the monitored area per pixel is usually given as $\frac{(\mu\text{m})^2}{pixel}$. However, the area is not given from this experiment, only the side of a square (pixel). The experimental calibration is measured with the help of a ruler with a known distance between two lines that is placed in the sample position of the setup. Two lines are drawn to mark the desirable distance to be measured, as illustrated in figure 5 by the distance between two lines on the ruler. The distance is known in μm and the pixel size is known (2.3× 2.3 μm). By counting the pixels in the images and dividing it by the distance between the two lines the pixel/μm value is given. In the case of this experiment, the chip is more rectangular in size. The number of pixels multiplied by the value for the calibration gives the field of view of the microscope.

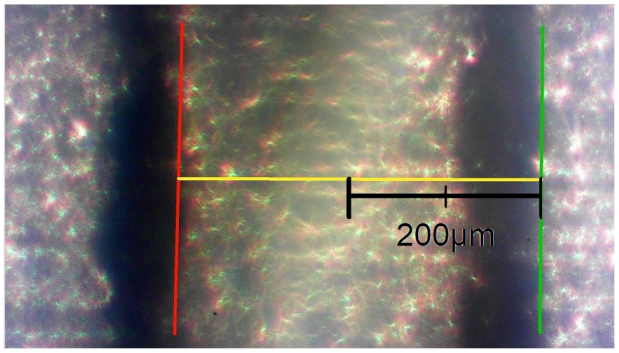

Figure 5: The red and green lines are placed manually in the desirable position. The yellow line marks the distance that is to be measured. The scale is representative of the distance between the lines on the ruler.

3.3 Laser spot size

The laser beam spot size is measured as the full width half maximum (FWHM). The spot size is measured using a bare camera (i.e. without any optics) in the sample position that detects the laser beam spot. The computer displays the image shown in figure 6. The FWHM of the curve is derived by fitting a Gaussian to the intensity curve of the beam spot with help of the software and data from from the plots (see fig 7) using the formula:

$$y = y_0 + \frac{A}{w\sqrt{\frac{\pi}{2}}} \cdot e^{-2\frac{(x-x_c)^2}{w^2}} \tag{14}$$

which is correlated to equation 12. Here A is the area under the curve, w is the width of the curve, and x_c denotes the center of the Gaussian curve. Once the Gaussian curve is fitted, the full width half maximum (FWHM) value can be derived. This values indicated the spot width.

The FWHM is used when deriving the $\frac{1}{e^2}$ diameter for the Gaussian curve. This diameter is about 1.7 times larger than the FWHM [20].

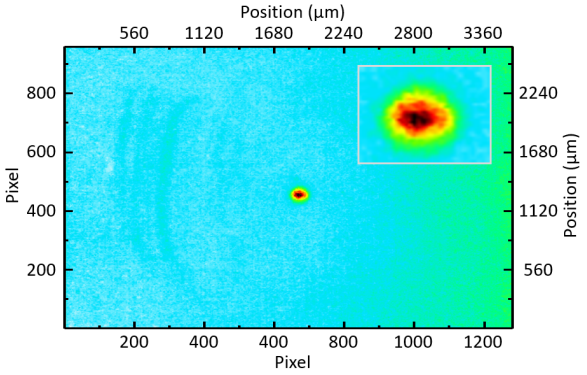

Figure 6: The spot size of the laser as provided by the camera. The inset is a zoomed in view of the actual spot. The bottom and left axis give the pixel number as read out by the camera. The top and right axis give the position on the camera chip calculated from the pixel number and the pixel size.

3.4 Laser throughput

The power of the laser is measured by replacing the sample chamber with an power meter. To account for reflection on the entrance window of the sample chamber, the window is placed on top of the power meter during the measurements. The output power of the laser is then tuned by variation of the driving current. The voltage is set and the current is self-limited by the laser diode. The power is used to calculate the intensity, which in turn is used to derive the field strength.

Table 1: Measurements of the infrared laser in order to calculate the intensity of the laser spot.

Voltage (V)	Current (mA)	Power (W)
1.44	277	0.005
1.46	300	0.021
1.51	398	0.115
1.56	498	0.200
1.62	596	0.310
1.67	695	0.400
1.73	797	0.500
1.78	895	0.600
1.85	994	0.700
1.88	1094	0.800
1.93	1194	0.880

4 Results

In this chapter all the results from the characterization of the setup will be presented. These results include the calibration of the microscope, the laser output power and spot size on the sample position.

4.1 Calibration

The distance between two lines on the ruler was measured to be ~1141 pixels, corresponding to 666 μm.

The calibration: $C = \frac{666}{1141}\frac{\mu\text{m}}{\text{pixels}} = 0.5837\frac{\mu\text{m}}{\text{pixels}}$

The inverse value for the calibration: $C^{-1} = \frac{1141}{666}\frac{\text{pixels}}{\mu\text{m}} = 1.71326\ \frac{\text{pixels}}{\mu\text{m}}$

4.2 Field of view

The experimental value for the field of view is derived from the amount of pixels on the camera (1920×1080) and the μm/pixel that is measured:

$$(1920 \cdot 0.5837) \times (1080 \cdot 0.5837)\ \mu\text{m}$$

$$= 1.120 \times 0.630\ \text{mm}$$

The theoretical values for the magnification V and field of view are:

$$\text{f}_1 = 4, \text{f}_2 = 15\ \text{cm} \Rightarrow V = \frac{15}{4} = 3.75$$

The theoretical field of view is given from the calculations found in section 3.1:

$$\Rightarrow 1.2 \times 0.93\ \text{mm}$$

The numerical aperture for the setup is $NA \approx 0.3$. This value is only theoretical since it cannot be derived experimentally.

4.3 Laser spot size

The full width half maximum (FWHM) of the curve is calculated with Origin from the graphs in fig 7.

Result of FWHM given from measurement data (including the $\frac{1}{e^2}$-value mentioned in the theory):

$$\text{FWHM} = 138.81269\ \mu\text{m}$$

$$\frac{1}{e^2} = 1.7 \cdot \text{FWHM} = 235.981573\ \mu\text{m}$$

The spot size area is then 60535 $\mu\text{m}^2 = 0.00060535\ \text{cm}^2$

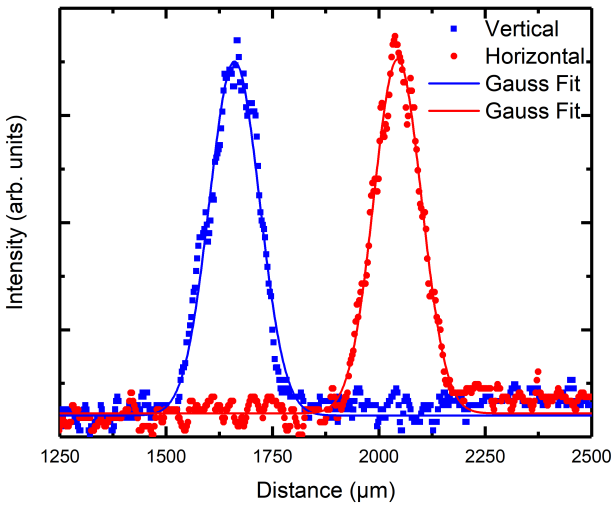

Figure 7: The curves of the spot size and their respective Gaussian fits.

4.4 Laser throughput

The results for the intensities and are presented in table 2 below.

Table 2: Intensities and the corresponding field strengths as derived from the values measured for the power.

Power (W)	Intensity (W/cm^2)	Field strength (V/cm)
0.005	8.260	78.890
0.021	34.691	161.673
0.115	189.972	387.334
0.200	330.386	498.932
0.310	512.098	621.1165
0.400	660.772	705.596
0.500	825.965	788.880
0.600	991.158	864.175
0.700	1156.351	933.416
0.800	1321.544	997.863
0.880	1453.699	1046.568

4.5 Laser deposition of the amorphous nonlinear medium

Laser deposition is a useful method to generate thin coatings. The laser hits the glass slide with the sample (shown in red in figure 8) placed on the opposite site. The sample evaporates, shown as the yellow triangular shape in the figure). This evaporation a forms a thin coating on top of the LED.

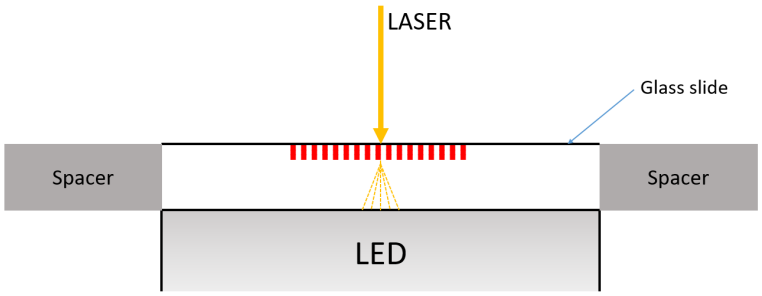

Figure 8: Model of laser deposition on an LED using a (pulsed) laser. The sample is shown in red and the evaporation is shown as the yellow triangle below the sample.

A small portion of the sample is placed onto a cover glass. This cover glass is then placed in a fixed position inside of the sample chamber. Another glass cover glass plate is attached inside the sample chamber with some distance to the one carrying the sample, forming an enclosed space between the two plates of glass. The cover glass with the powder is facing down towards the clean cover glass. The sample chamber is evacuated using a small vacuum pump that ensures a pressure in the low mBar range. The laser power is adjusted so that the powder gets heated up and evaporates from the cover glass. The laser beam is moved across the whole sample. The documentation of the sample throughout the laser deposition process is shown in figure 9. Thereafter the cover glass with the evaporation is examined to check for white light emission when irradiated with the laser. The white light emission from the sample can be seen in figure 10. If white light was not found on

the thin film after laser deposition has been performed, the cover glass could be coated a second time. The thin film might have to be thicker in order to produce white light.

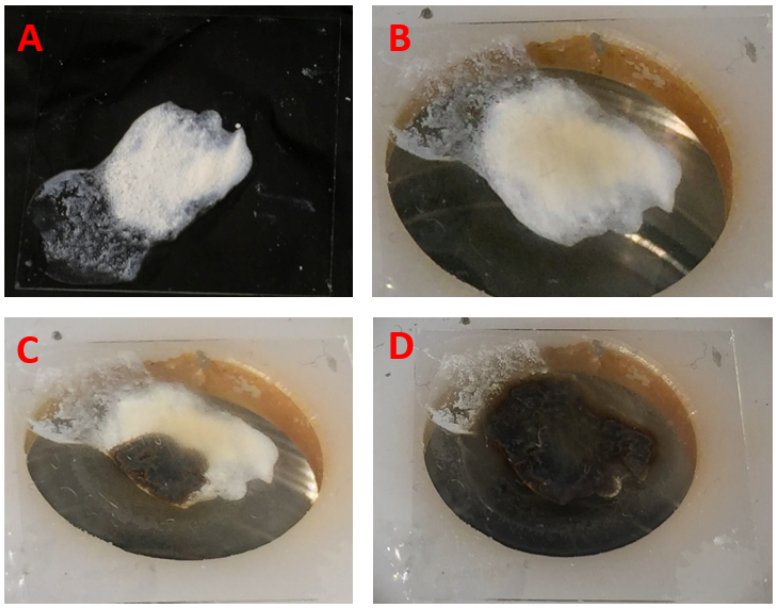

Figure 9: Sample on which laser deposition was performed. A) Prepared sample. B) Sample placed in sample chamber. C) Sample irradiated by the laser. The black spot indicated the evaporated area. D) The entire sample has been irradiated with the laser.

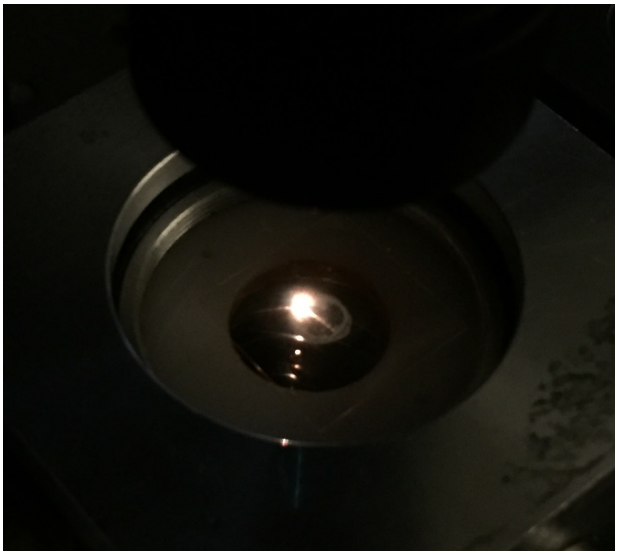

Figure 10: White light emitted by the sample during irradiation of infrared laser light.

5 Outlook

5.1 Summary

In summary, theoretical knowledge of light-matter interaction and nonlinear physics of nonlinear physics has been presented. A confocal setup was designed and assembled. This setup was later tested using various methods in order to characterize it. The different aspects of the setup characterized were the magnification, field of view, calibration and spot size. As a final test, laser deposition was performed on a small sample of the amorphous nonlinear medium $(PhSn)_4S_6$.

Some suggested improvements include using a ruler with sharper, more distinct lines to improve the calibration results by having a greater accuracy. To measure the resolution, or resolving power, of the microscope a set of objects placed at decreasing distance from each other would be needed. Due to lack of access to such a target the measurements were not done in this project. The experimental

field of view is observed to be smaller than the theoretical, and the experimental value for the resolving power is smaller as well. This could be a result of the microscope not being able to distinguish the correct pixel size, thus making the values somewhat unreliable in accuracy.

The magnification of the setup could be improved. The experimental value is not the same as the theoretical value, therefore it is assumed that the camera have not done ideal measurements.

The fact that it was possible to perform a Gaussian fit with nearly identical results for horizontal and vertical axis assures that the shape of the beam is Gaussian. For this experiment only one type of molecule is studied in its powdered state due to time restriction. Investigating more materials would require more time, but would perhaps be suited for a potential master's thesis and project.

Acknowledgements

First and foremost, I would like to thank Nils Rosemann, my supervisor throughout this project. Without your help, guidance and patience this thesis would not have been written. I also want to thank Rasmus Westerström for taking his time to give me feedback and guide me along the way of producing this thesis. A special thank you goes out to the Division of Chemical Physics at the Chemistry Department for hosting me, and to the people there whom I am very grateful to have met and talked to.

Last, but not least, I would like thank my parents for supporting me throughout these three years that I have studied physics, and encouraging me to not give up when things got hard.

References

[1] Maiman TH. The Laser Inventor - Memoirs of Theodore H. Maiman. 2nd ed. Switzerland: Springer Biographies; 2017 [cited 22-04-2018]. 245-253 p. ISBN: 978-3-319-61939-2. doi: 10.1007/978-3-319-61940-8

[2] Ajlal S, Sohail Zafar M, Khurshid Z, Najeeb S. Applications of Light Amplification by Stimulated Emission of Radiation (Lasers) for Restorative Dentistry. Karger Med Princ Pract.. 2016 [cited 2018 Apr 26]; 25 (3): 201–11. doi: 10.1159/000443144

[3] Bell S. A Dictionary of Forensic Science [Internet]. 1st ed. Oxford University Press; 2012 [cited 2018 Apr 26]. 303 p. Available from: `https://books.google.com/books?id=P1hEpzq-9HIC&pgis=1`

[4] Alfano RR. The Supercontinuum Laser Source Internet] : Fundamentals with Updated References. Second Edition. New York, NY: Springer Science+Business Media, Inc.; 2006.

[5] "Laser Facts". Nobelprize.org. Nobel Media AB 2014. [Internet]. [cited 23-04-2018]. Available from: `http://www.nobelprize.org/educational/physics/laser/facts/use.html`

[6] New, G. Introduction to Nonlinear Optics. Cambridge: Cambridge University Press; 2011.

[7] Siwach P, Kumar A, Saini TS. Broadband supercontinuum generation spanning 1.5–13 μm in Ge11.5As24Se64.5 based chalcogenide glass step index optical fiber. Opt - Int J Light Electron Opt [Internet]. 2018 Mar 1 [cited 2018 May 2];156:564–70. Available from: `https://www.sciencedirect.com/science/article/pii/S0030402617316194?via%3Dihub`

[8] Dudley J. M. Genty G, Coen S. Supercontinuum generation in photonic crystal fiber. Rev Mod Phys [Internet]. 2006 Oct 4 [cited 2018 Apr 23];78(4):1135–84. doi: 10.1103/RevModPhys.78.1135

[9] Rosemann, N. W., Eußner JP, Beyer A, Koch SW, Volz K, Dehnen S, et al. A highly efficient directional molecular white-light emitter driven by a continuous-wave laser diode. Science [Internet]. 2016 Jun 10 [cited 2018 Apr 25];352(6291):1301–4. Available from: `http://www.ncbi.nlm.nih.gov/pubmed/27284190`

[10] Rosemann NW, Eußner JP, Dornsiepen E, Chatterjee S, Dehnen S. Organotetrel Chalcogenide Clusters: Between Strong Second-Harmonic and White-Light Continuum Generation. J Am Chem Soc [Internet]. 2016;138(50):16224–7. doi: 10.1021/jacs.6b10738

[11] Klingshirn, C. F. Semiconductor Optics. 4th ed. Berlin, Heidelberg: Springer; 2012 ISBN 978-3-642-28361-1. doi: 10.1007/978-3-642-28362-8

[12] Boyd, R. W., Nonlinear Optics -. Academic Press. 3rd ed. Amsterdam, Boston: Elsevier; 2008. ISBN: 978-0-12-369470-6

[13] Mills, D. L. Nonlinear Optics - Basic Concepts. 2nd ed. Berlin, Heidelberg: Springer; 1991. ISBN: 3-540-54192-6

[14] Griffiths, D. J., Introduction to Electrodynamics. 4th ed. Smith J, editor. Vol. 73, American Journal of Physics. Pearson; 2013. 623 p.

[15] Rosemann, N. W., Functionalization of Inorganic Semiconductors by Advanced Nanostructures. University of Malburg; 2016.

[16] Chemla, D. S., Zyss, J., Chapter II-1 – Quadratic Nonlinear Optics and Optimization of the Second-Order Nonlinear Optical Response of Molecular Crystals.

In: Nonlinear Optical Properties of Organic Molecules and Crystals. 1987. p. 23–191.

[17] Wilson, M. 2 Dec 2016. Microscope Resolution: Concepts, Factors and Calculation. Leica Microsystems. Available from: https://www.leica-microsystems.com/science-lab/microscope-resolution-concepts-factors-and-calculation/

[18] Keyence. What is a laser scanning confocal microscope?. Main Types of Microscopes: Types & Principle [Internet]. Keyence Corporation; 2018. [cited 03-05-2018] Available from: https://www.keyence.com/ss/products/microscope/bz-x700/study/principle/002/c_laser.jsp?iframe=true&width=800&height=550

[19] Peatross J, Ware M. Physics of Light and Optics. 2008 [cited 2018 May 3]; 236 p. Available from: http://optics.byu.edu/BYUOpticsBook_2008.pdf

[20] Hill, D. 4 April 2007. How to Convert FWHM Measurements to 1/e-Squared Halfwidths. Radiant Zemax Knowledge Base. Available from: http://customers.zemax.com/os/resources/learn/knowledgebase/how-to-convert-fwhm-measurements-to-1-e-squared-ha

[21] Rosemann, N. Scanning Setup Drawing [Private Source]. 2018 [cited 26-02-2018].

[22] Amorim Garcia Filho, C. A., Yehoshua, Z., Gregori, G., Puliafito, C. A., Rosenfeld, P. J.. Optical Coherence Tomography. In: Ryan, S. J., editor. Retina. Fifth edition. Elsevier; 2013. p. 82-110